RSC Advances

PAPER

View Article Online
View Journal | View Issue

Check for updates

Cite this: *RSC Adv.*, 2017, **7**, 41111

Significantly enhanced thermoelectric performance of Cu-doped p-type $Bi_{0.5}Sb_{1.5}Te_3$ by a hydrothermal synthesis method†

Zichen Wei,[ab] Chenyang Wang,[a] Li You,[a] Shijie Zhao,[ab] Kang Yang,[b] Haiyan Chen,[*b] Jun Luo[*a] and Xiaoyuan Chen[b]

Cu-doped p-type $Bi_{0.5}Sb_{1.5}Te_3$ compounds have been prepared by a facile hydrothermal method. X-ray powder diffraction analysis shows that the lattice parameter decreases with the Cu content, indicating that Cu^+ ions are distributed on the crystal site of Bi/Sb, which is further confirmed by the p-type conducting behavior of the Cu-doped $Bi_{0.5}Sb_{1.5}Te_3$. With the addition of Cu, the hole carrier concentration increases, and meanwhile the lattice thermal conductivity decreases. Furthermore, the greatly raised hole carrier concentration effectively suppresses the bipolar effect, which is beneficial for improving the thermoelectric properties. A dimensionless thermoelectric figure of merit (*ZT*) value of ~1.2 at room temperature is achieved for the sample with 0.6 wt% Cu (nominal composition), and the *ZT* value increases with the temperature to ~1.5 at 150 °C. Cu-doped $Bi_{0.5}Sb_{1.5}Te_3$ samples exhibit most excellent thermoelectric performance among the presently available $(Bi,Sb)_2Te_3$-based materials, implying great potential as near room temperature thermoelectric materials.

Received 5th June 2017
Accepted 18th August 2017

DOI: 10.1039/c7ra06277j

rsc.li/rsc-advances

Open Access Article. Published on 23 August 2017. Downloaded on 2/13/2026 10:14:08 AM.
This article is licensed under a Creative Commons Attribution-NonCommercial 3.0 Unported Licence.

Introduction

With the progress and development of human society, energy shortage has been a crisis issue nowadays. Thermoelectric materials are environmentally friendly energy-saving materials, which can directly convert heat into electricity (Seebeck effect) or *vice versa* (Peltier effect).[1,2] The conversion efficiency of a thermoelectric device is measured by the dimensionless thermoelectric figure of merit (*ZT*) of the material

$$ZT = S\sigma^2 T/\kappa, \quad (1)$$

where S is the Seebeck coefficient, σ electrical conductivity, κ thermal conductivity, and T the absolute temperature. For practical applications, thermoelectric materials with high *ZT* values are greatly desired.

Bi_2Te_3-based materials[3–9] are classical room-temperature thermoelectric materials. Both p-type $(Bi_xSb_{1-x})_2Te_3$ (ref. 10 and 11) and n-type $Bi_2Se_{3-y}Te_y$ (ref. 6 and 12–14) present excellent thermoelectric performance and have been put into commercial applications, which are well known as the most efficient thermoelectric materials operating near room temperature.[15,16] According to literature reports, the $Bi_{0.5}Sb_{1.5}Te_3$ alloy possesses the highest *ZT* value in all $Bi_{2-x}Sb_xTe_3$ solid solutions.[17,18] Many methods have been attempted to fabricate Bi_2Te_3-based materials, *e.g.* ball milling,[19–21] sintering[22,23] and hot deformation.[24–27] However, sample preparation needs a long time by most of the synthesis methods.[17,28–31] Instead, hydrothermal synthesis as an effective method to fabricate Bi_2Te_3-based materials takes much shorter time,[32,33] while the synthesis of a single-phase $Bi_{0.5}Sb_{1.5}Te_3$ solid solution by hydrothermal reaction is rarely reported.[18,34,35] Furthermore, the reported room-temperature thermoelectric properties of the Bi_2Te_3-based alloy synthesized by the hydrothermal method are not as good as expected.[18,35,37] Therefore, it is desirable to develop a facile hydrothermal method to prepare an ideal single-phase $Bi_{0.5}Sb_{1.5}Te_3$ alloy with optimized thermoelectric properties.

In this work, Cu-doped $Bi_{0.5}Sb_{1.5}Te_3$ samples have been prepared by a facile hydrothermal method. According to the result of structure analysis, single-phase alloys with excellent thermoelectric properties have been successfully synthesized. A room-temperature *ZT* value as high as ~1.2 has been achieved for the sample doped with nominal 0.6 wt% Cu, and its maximum *ZT* value of ~1.5 is obtained at 423 K. To our knowledge, the nominal 0.6 wt% Cu-doped $Bi_{0.5}Sb_{1.5}Te_3$ sample synthesized by a hydrothermal method in our experiments exhibits the most excellent thermoelectric performance among the presently available $(Bi,Sb)_2Te_3$-based materials, showing the great potential as near room temperature thermoelectric material.

[a]*School of Materials Science and Engineering, Shanghai University, Shanghai 200444, China. E-mail: junluo@shu.edu.cn*

[b]*Thin Film Optoelectronic Technology Center, Shanghai Advanced Research Institute, Chinese Academy of Sciences, Shanghai 201210, China. E-mail: chenhy@sari.ac.cn; Tel: +86 21 20350846*

† Electronic supplementary information (ESI) available. See DOI: 10.1039/c7ra06277j

Open Access Article. Published on 23 August 2017. Downloaded on 2/13/2026 10:14:08 AM.
This article is licensed under a Creative Commons Attribution-NonCommercial 3.0 Unported Licence.

Experimental

All samples were prepared *via* a facile hydrothermal method. High-purity powders of $SbCl_3$ (Adamas 99%), $BiCl_3$ (Adamas 99%+), Te (Adamas 99.999%) and Cu (Adamas 99.9%) were weighed according to stoichiometric $Bi_{0.5}Sb_{1.5}Te_3$ + x wt% Cu (x = 0.0, 0.6, 1.6, 2.6). In a polytetrafluoroethylene (PTFE) cylindrical container, the raw materials were dissolved in deionized water with the aid of ultrasonication. Organic complexing additive ethylene diamine tetraacetic disodium salt (Greagent ≥ 99%) and the dispersant N_2H_4 (Adamas 80% Aq.) were added to previous solution. Then the pH value of the solution was adjusted to 11 by adding NaOH (Greagent ≥ 96%). The final filling ratio of solution inside the PTFE container is up to 80%. After 1 h of ultrasonication at room temperature, the PTFE container with the solution was transferred into a drying oven with a vacuum chamber and then heated at 180 °C for 48 h. The obtained powders were washed by the de-ionized water and then dried at 70 °C for 5 h. The obtained samples were marked as S1 (x = 0), S2 (x = 0.6), S3 (x = 1.6) and S4 (x = 2.6), respectively. For thermoelectric measurement, as-prepared powders were hot pressed at 350 °C for 30 minutes to acquire pellets.

X-ray powder diffraction (XRD) patterns were collected on a Bruker AXS D8 Advance Diffractometer with Cu Kα radiation (λ = 0.154056 nm) using the continuous scanning method with a scanning voltage of 40 kV and a scanning speed of 0.01° per step. The morphologies of the samples were observed on a Hitachi S-4800 scanning electron microscope (SEM). LSR-3/1100 thermoelectric measurement system was used to measure the Seebeck coefficient and resistivity. The thermal diffusivity of the sample was detected by a laser flash diffusivity method on a Netzsch Laser Flash Apparatus (LFA) 1000. The total thermal conductivity κ was calculated by the equation $\kappa = D\rho C_p$, where D, ρ and C_p were the thermal diffusivity, the mass density and the volumetric specific capacity of the sample, respectively. C_p was measured by a Netzsch differential scanning calorimetry (DSC) 201F1 instrument, and ρ by the Archimedes-method.

Results and discussion

Fig. 1 shows the XRD patterns of the samples S1–S4. The sample S4 with nominal 2.6 wt% Cu can be solely indexed to a single phase of rhombohedra $Bi_{0.5}Sb_{1.5}Te_3$ (PDF#49-1713). For the samples S1, S2 and S3, only a trace amount of unknown second phase appears as the impurities, indicating that the Cu-doped $Bi_{0.5}Sb_{1.5}Te_3$ solid solution as the main phase has been successfully synthesized. There are three kinds of possible positions for Cu ions in the crystal structure of $Bi_{0.5}Sb_{1.5}Te_3$, namely, lattice site, interstitial site and interlayer position. If Cu^+ enters the interstitial site or interlayer position, the lattice constant should increase with the Cu content. However, as shown in Table 1, the lattice constant a of the Cu-doped $Bi_{0.5}Sb_{1.5}Te_3$ samples decreases with the Cu concentration. Therefore, the decrease of the lattice constant a can be attributed to the partial replacement of Bi^{3+}/Sb^{3+} by Cu ions because the

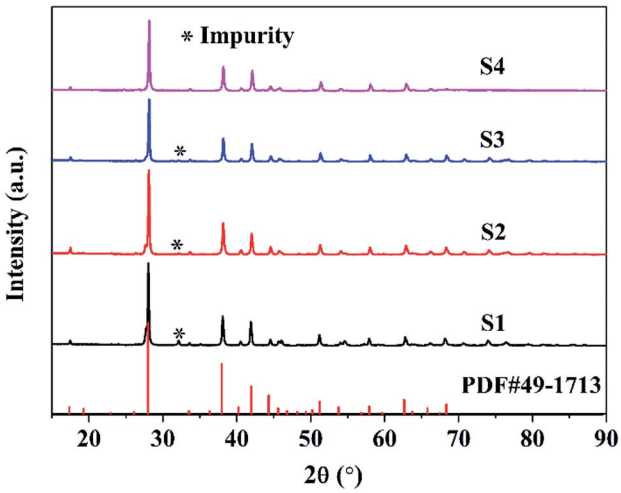

Fig. 1 XRD patterns of the samples S1–S4. (Nominal Cu contents of S1, S2, S3 and S4 are 0 wt%, 0.6 wt%, 1.6 wt% and 2.6 wt%, respectively).

radius of Cu^+ (0.77 Å) is smaller than the average radius of Bi^{3+}/Sb^{3+} (1.03/0.76 Å). On the other hand, for the Cu-doped samples, the c-axis parameter remained nearly constant within the standard deviations as the Cu content increases, implying that Cu ions only replace Bi^{3+}/Sb^{3+} but not go to the interlayer position. The crystal site of Cu ions in the structure can be further verified by the Hall effect measurement. According to Hall effect measurement, the Cu-doped $Bi_{0.5}Sb_{1.5}Te_3$ samples show p-type conducting behavior. Fig. 2 shows the dependence of the carrier concentration on the Cu content for all $Bi_{0.5}Sb_{1.5}Te_3$ samples. The hole concentration increases with the Cu doping content, indicating that the Cu^+ ion, acting as an acceptor, enters the lattice to replace part of Bi^{3+}/Sb^{3+} ions, which is consistent with the conclusion reported by Hao *et al.*[38] Otherwise, the Cu-doped $Bi_{0.5}Sb_{1.5}Te_3$ samples should exhibit n-type conducting behavior if the Cu^+ ion goes into the interstitial site or interlayer position.

To further explore the structural feature of Cu-doped $Bi_{0.5}Sb_{1.5}Te_3$, the morphologies of the as-prepared powder and hot-pressed bulk sample have been observed by SEM. Fig. 3a and b show the SEM images of sample S3, exhibiting the feature of small particle sizes. As shown in Fig. 3a, most of the particles are at the nanoscale, typically on the order of several hundreds of nanometers. Furthermore, some mesoscale hexagonal platelets with the particle sizes from 1 to 10 micrometers are observed in Fig. 3a, which should relate to the anisotropic crystal structure of $Bi_{0.5}Sb_{1.5}Te_3$. The Bi_2Te_3 compound has a rhombohedra structure[32] with the space group $R\bar{3}m$, wherein along the c-axis, the atomic layers array in the order of –Te(1)–Bi–Te(2)–Bi–Te(1)– and the neighboring Te(1) layers are linked by weak van der Waals bonds.[34–37] Therefore, the morphology of Bi_2Te_3-based alloy normally exhibits the feature of hexagonal platelets. For the powders obtained in our work, under the control of hydrothermal synthesis, most of grains are nanoparticles with deficient crystallinity, while only a small number of grains are well-crystallized, existing as hexagonal platelets. This could also explain the isotropic properties of these samples

 This journal is © The Royal Society of Chemistry 2017

Open Access Article. Published on 23 August 2017. Downloaded on 2/13/2026 10:14:08 AM.
This article is licensed under a Creative Commons Attribution-NonCommercial 3.0 Unported Licence.

Table 1 Lattice constant of undoped and Cu-doped $Bi_{0.5}Sb_{1.5}Te_3$

Samples	Nominal Cu content x (wt%)	a (Å)	c (Å)	V (Å^3)
S1	0	4.3094 (±0.0016)	30.487 (±0.0007)	490.31 (±0.0020)
S2	0.6	4.3015 (±0.0011)	30.473 (±0.0006)	488.31 (±0.0015)
S3	1.6	4.2986 (±0.0018)	30.466 (±0.0009)	487.53 (±0.0025)
S4	2.6	4.2914 (±0.0024)	30.473 (±0.0011)	486.00 (±0.0030)

(see Fig. S1 and S2†). As shown in Fig. 3b, the small particle size is maintained after hot pressing (the feature of small particle size can also be observed from the cross section of the bulk, shown in Fig. S3†). Hence, the small particle size as well as numerous grain boundaries of the samples synthesized by the hydrothermal method could contribute to the reduced lattice thermal conductivity around room temperature, which is beneficial for the Cu-doped $Bi_{0.5}Sb_{1.5}Te_3$ aiming at room-temperature applications.

Fig. 4 shows the electrical transport properties of the undoped and Cu-doped $Bi_{0.5}Sb_{1.5}Te_3$ samples. As shown in Fig. 4a, the Seebeck coefficients of all the samples are positive, further confirming their p-type conducting behavior. The room-temperature Seebeck coefficient decreases with the Cu content because of the increased carrier concentration. For the undoped sample S1, its Seebeck coefficient decreases with the increasing temperature, which can be ascribed to the bipolar effect caused by the intrinsic excitation below room temperature.[30,35] For the Cu-doped samples S2–S4, their room temperature Seebeck coefficients decrease with the increase of Cu content, which can be attributed to increased hole concentration by substituting of Cu for Bi/Sb. Furthermore, their temperature-dependent Seebeck coefficients show the typical behavior of a degenerate semiconductor. As shown in Fig. 4a, for samples S2–S4, the Seebeck coefficient firstly increases linearly with the increasing temperature, but linear trend of the Seebeck curve is suppressed by the bipolar effect at elevated temperature. It is obvious that the bipolar effect of the Cu-doped samples shifts to higher temperature because the mixed conduction is suppressed by increasing hole concentration. Thus, comparing with the undoped sample, the Seebeck coefficients of the Cu doped samples increase dramatically in the temperature range of 150–350 °C.

As shown in Fig. 4b, the temperature-dependent electrical conductivity of the undoped sample S1 also shows the conducting behavior of intrinsic excitation, *i.e.* the electrical conductivity increases with the increasing temperature. For the Cu-doped samples, their electrical conductivities firstly decrease rapidly with the raised temperature, and then decrease slowly with the temperature due to the mixed conduction. The slowly decrease of electrical conductivity at high temperature for all the samples can be ascribed to the bipolar effect. Furthermore, the doping of Cu increases the hole concentration, which effectively suppresses the bipolar effect and shifts the intrinsic excitation temperature to higher temperature. It is worth to note that the σ values of the Cu-doped samples prepared *via* a facile hydrothermal method in our work could be comparable to that of Bi–Sb–Te alloys synthesized by conventional sintering methods,[30,39] indicating this facile hydrothermal method is an effective route for developing high-performance $(Bi,Sb)_2Te_3$-based materials.

It should be pointed out that the room-temperature electrical conductivity is almost the same for the samples S2 and S3. To clarify this, Hall carrier concentration and mobility have been measured. As listed in Table 2, the hole concentration of sample S3 is almost twice of that of the sample S2, while its mobility is nearly half of that of the latter one. Hence, these two samples have similar electrical conductivity at room temperature. The reduced carrier mobility of the sample S3 could be ascribed to the enhanced carrier scattering in two aspects: (1) more lattice point defects produced by Cu substitution and (2) increased hole concentration.

The combination of raised Seebeck coefficient and increased electrical conductivity results in a power factor of ~25 μW cm^{-1} K^{-2} at 50 °C for sample S2 (Fig. 5), which is

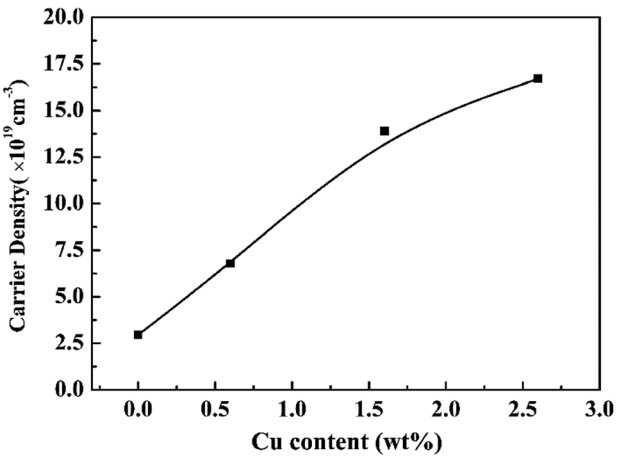

Fig. 2 Room-temperature hole carrier concentration as a function of the nominal Cu content for all $Bi_{0.5}Sb_{1.5}Te_3$ samples.

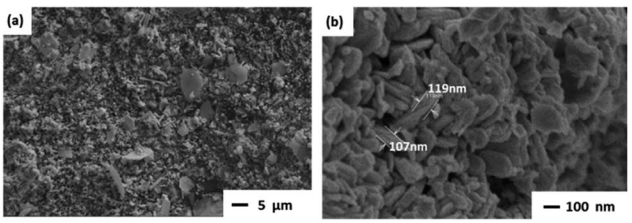

Fig. 3 Typical SEM images of (a) the as-prepared powders and (b) ground powders after the hot pressing of sample S3.

Open Access Article. Published on 23 August 2017. Downloaded on 2/13/2026 10:14:08 AM.
This article is licensed under a Creative Commons Attribution-NonCommercial 3.0 Unported Licence.

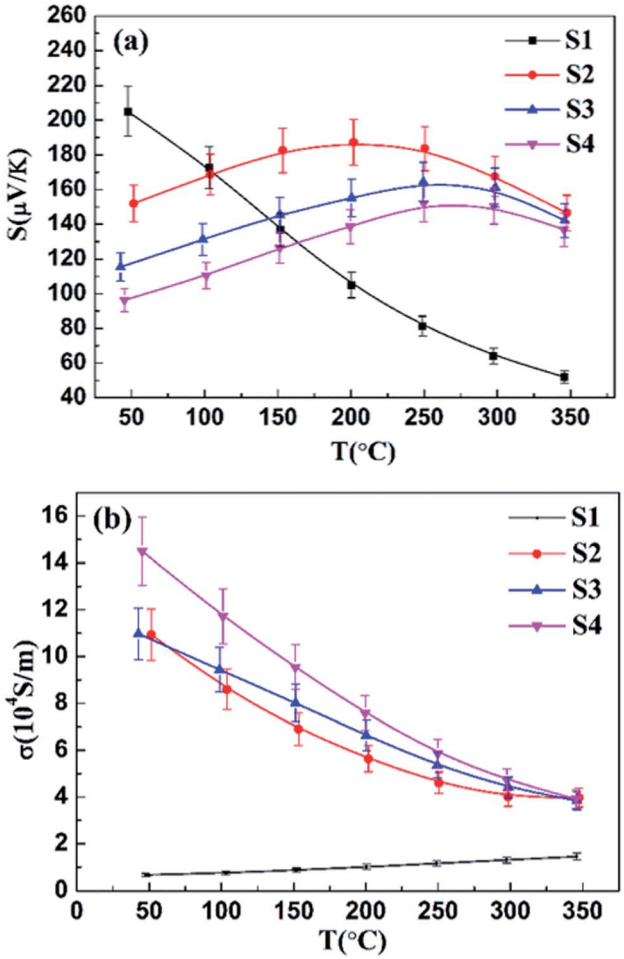

Fig. 4 Temperature-dependences of (a) Seebeck coefficient and (b) electrical conductivity of undoped and Cu-doped samples.

nearly 9 times as large as that of sample S1. The power factor decreases to 23 μW cm^{-1} K^{-2} at 150 °C and remains as high as ~8.5 μW cm^{-1} K^{-2} at 350 °C for sample S2. Furthermore, the power factors of Cu-doped samples are always much larger than that of undoped sample in the measured temperature range from 50 °C to 350 °C.

Fig. 6 shows the temperature-dependent thermal conductivity of samples S1–S4. It is obvious that all the samples have very low thermal conductivities. As shown in Fig. 6, the thermal conductivity of sample S1 increases with the increasing temperature, which could be ascribed to the increased electronic contribution to the total thermal conductivity caused by the bipolar effect. Similarly, for the Cu-doped samples, the increase of the thermal conductivity at

Table 2 Carrier concentration (n) and mobility (μ) of S2 and S3

Samples	Nominal Cu content x (wt%)	n (10^{19}/cm^3)	μ (cm^2 V^{-1} s^{-1})
S2	0.6	6.7792	60.7478
S3	1.6	13.9000	29.2516

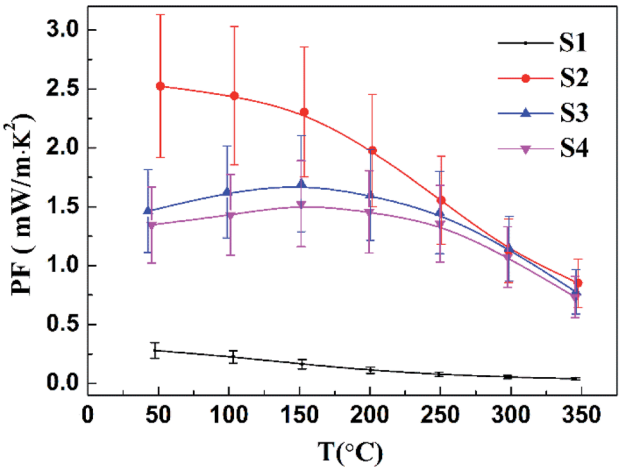

Fig. 5 Power factor as a function of temperature for undoped and Cu-doped samples.

high temperature can also be attributed to intrinsic excitation.

The thermal conductivity of Cu-doped samples S2–S4 is higher than that of the undoped sample S1 owing to the dramatically increased electronic thermal conductivity, since the hole concentration is significantly enhanced with the Cu content.

For undoped sample S1, compared with those synthesized by mechanical alloying[19] and spark plasma sintering (SPS),[39] its nanostructuring obtained by hydrothermal synthesis lowers the thermal conductivity by about 31–50% at room temperature, due to the contribution of additional phonon scattering, implying that our hydrothermal synthesis method is effective on reducing the thermal conductivity. As for sample S2, its average thermal conductivity in the temperature range of 150–350 °C is about 0.71 W m^{-1} K^{-1}, approximately 12%, 21% and 22% reduction than those of Cu-doped Bi–Sb–Te samples reported by Lee *et al.*,[17] Hao *et al.*[38] and Cui *et al.*,[30] respectively. The low thermal conductivity of sample S2 can be ascribed to

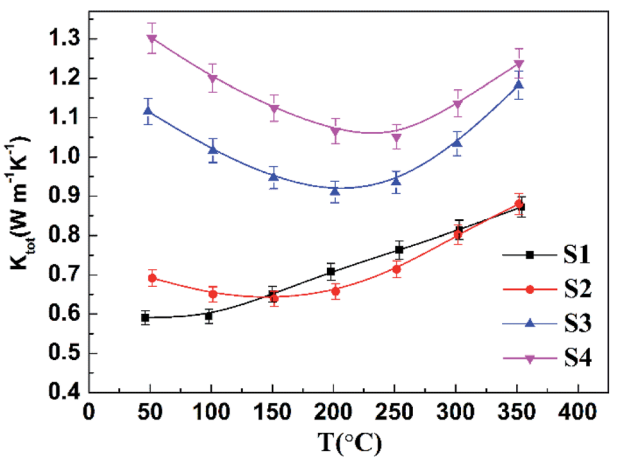

Fig. 6 Temperature-dependent thermal conductivity for undoped and Cu-doped samples.

This journal is © The Royal Society of Chemistry 2017

Open Access Article. Published on 23 August 2017. Downloaded on 2/13/2026 10:14:08 AM.
This article is licensed under a Creative Commons Attribution-NonCommercial 3.0 Unported Licence.

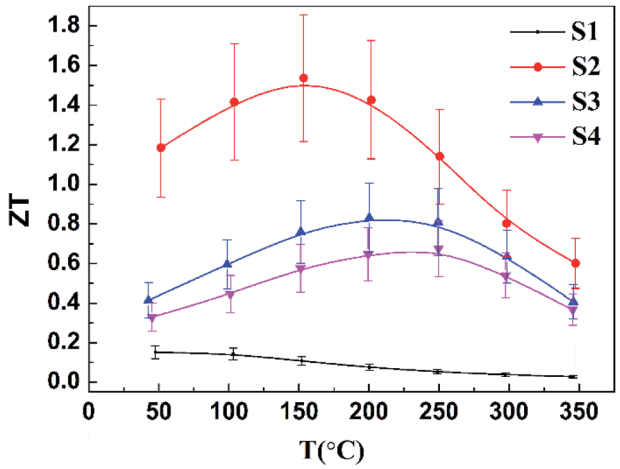

Fig. 7 Temperature dependence of *ZT* values for undoped and Cu-doped samples.

different defects: nanoscale grains by hydrothermal synthesis, atomic-scale point defects of Cu substitution for Bi^{3+}/Sb^{3+}, and the presence of second phase. It is worth to note that, in p-type $Bi_{0.5}Sb_{1.5}Te_3$ materials, the Cu dopants not only increase the hole concentration, but also introduce nanostructural defects, which were also observed in SPS-treated Cu-doped $Bi_{0.5}Sb_{1.5}Te_3$ bulk samples.[38]

Fig. 7 presents the *ZT* values for the undoped and Cu-doped samples. The *ZT* value of sample S1 decreases with the increasing temperature, which can be explained by a drastic reduction of the Seebeck coefficient due to the bipolar effect. The doping of Cu effectively suppresses the bipolar effect by increasing the hole concentration, leading to a shift of the peak *ZT* value to higher temperature with the raised Cu concentration. Obviously, the *ZT* values of the samples with Cu doping are much larger than those of the undoped sample, even though the total thermal conductivity is enhanced after the Cu doping. Therefore, the huge enhancement of *ZT* from 50 °C to 350 °C is mainly contributed from the power factor afforded by doping. However, with the further increased Cu content, the *ZT* value decreases, which probably originates from the increased electronic contribution to the thermal conductivity due to the increasing electrical conductivity. The sample with nominal 0.6 wt% Cu exhibits the best thermoelectric performance because of the appropriate doping level, small grain size, as well as the presence of trace amount of impurities. Finally, a *ZT* value of 1.2 around room temperature and a peak *ZT* value of ~1.5 at 150 °C are achieved for the sample S2. The average *ZT* value of sample S2 in the temperature range of 50–200 °C is about 1.4, ~40% improvement of that of the commercial Bi_2Te_3 ingot materials. It should be noted that, by the Cu doping, the optimum operating temperature is decreased and the working temperature range becomes broader, making Cu-doped bismuth antimony telluride based alloys have better prospects for commercial applications.

Conclusions

In this work, the Cu-doped p-type $Bi_{0.5}Sb_{1.5}Te_3$ compounds have been successfully synthesized by a facile hydrothermal method. Structural analysis indicates that the sample crystallizes into rhombohedra structure and the Cu^+ ions enter the crystal lattice by substituting partial Bi^{3+}/Sb^{3+}, which is further confirmed by the electrical properties measurement. The doping of Cu effectively suppresses the bipolar effect of $Bi_{0.5}Sb_{1.5}Te_3$ compound by increasing the hole concentration, leading to the improved electrical transport properties and increased power factor. The main contribution to the huge enhancement of *ZT* from 50 °C to 350 °C is the power factor afforded by Cu doping. The sample doped with nominal 0.6 wt% Cu shows a *ZT* value of ~1.2 around room temperature and a peak *ZT* value of ~1.5 at 150 °C, originating from the combined effect of appropriate doping level, small grain size, and the presence of uniformly dispersed trace amount of impurities.

Conflicts of interest

There are no conflicts of interest to declare.

Acknowledgements

This work was supported by National Natural Science Foundation of China (Grant No. 51201108, 11174308, 51371194, and 51632005) and Knowledge Innovation Project of the Chinese Academy of Sciences (Grant No. KGCX2-EW-315).

References

1 A. Majumdar, *Science*, 2004, **303**, 777–778.
2 J. Yang, L. Xi, W. Qiu, L. Wu, X. Shi, L. Chen, J. Yang, W. Zhang, C. Uher and D. J. Singh, *npj Comput. Mater.*, 2016, **2**, 15015.
3 Y. L. Chen, J. G. Analytis, J. H. Chu, Z. K. Liu, S. K. Mo, X. L. Qi, H. J. Zhang, D. H. Lu, X. Dai, Z. Fang, S. C. Zhang, I. R. Fisher, Z. Hussain and Z. X. Shen, *Science*, 2009, **325**, 178–181.
4 Y. Y. Li, G. Wang, X. G. Zhu, M. H. Liu, C. Ye, X. Chen, Y. Y. Wang, K. He, L. L. Wang, X. C. Ma, H. J. Zhang, X. Dai, Z. Fang, X. C. Xie, Y. Liu, X. L. Qi, J. F. Jia, S. C. Zhang and Q. K. Xue, *Adv. Mater.*, 2010, **22**, 4002–4007.
5 M. Scheele, N. Oeschler, K. Meier, A. Kornowski, C. Klinke and H. Weller, *Adv. Funct. Mater.*, 2009, **19**, 3476–3483.
6 H. Zhang, C.-X. Liu, X.-L. Qi, X. Dai, Z. Fang and S.-C. Zhang, *Nat. Phys.*, 2009, **5**, 438–442.
7 H. Goldsmid, *Materials*, 2014, **7**, 2577–2592.
8 F. Li, X. Huang, W. Jiang and L. Chen, *J. Electron. Mater.*, 2013, **42**, 1219–1224.
9 B. Poudel, *Science*, 2008, **320**, 634–638.
10 D. Kong, Y. Chen, J. J. Cha, Q. Zhang, J. G. Analytis, K. Lai, Z. Liu, S. S. Hong, K. J. Koski, S. K. Mo, Z. Hussain, I. R. Fisher, Z. X. Shen and Y. Cui, *Nat. Nanotechnol.*, 2011, **6**, 705–709.

Open Access Article. Published on 23 August 2017. Downloaded on 2/13/2026 10:14:08 AM.
This article is licensed under a Creative Commons Attribution-NonCommercial 3.0 Unported Licence.

11 W. Xie, S. Wang, S. Zhu, J. He, X. Tang, Q. Zhang and T. M. Tritt, *J. Mater. Sci.*, 2012, **48**, 2745–2760.
12 S. Wang, W. Xie, H. Li and X. Tang, *Intermetallics*, 2011, **19**, 1024–1031.
13 S. Wang, W. Xie, H. Li and X. Tang, *J. Phys. D: Appl. Phys.*, 2010, **43**, 335404.
14 W. Liu, K. C. Lukas, K. McEnaney, S. Lee, Q. Zhang, C. P. Opeil, G. Chen and Z. Ren, *Energy Environ. Sci.*, 2013, **6**, 552–560.
15 F. Hao, P. Qiu, Y. Tang, S. Bai, T. Xing, H.-S. Chu, Q. Zhang, P. Lu, T. Zhang, D. Ren, J. Chen, X. Shi and L. Chen, *Energy Environ. Sci.*, 2016, **9**, 3120–3127.
16 G. Tan, L. D. Zhao and M. G. Kanatzidis, *Chem. Rev.*, 2016, **116**, 12123–12149.
17 K.-H. Lee, H.-S. Kim, S.-I. Kim, E.-S. Lee, S.-M. Lee, J.-S. Rhyee, J.-Y. Jung, I.-H. Kim, Y. Wang and K. Koumoto, *J. Electron. Mater.*, 2012, **41**, 1165–1169.
18 C.-J. Liu, G.-J. Liu, C.-W. Tsao and Y.-J. Huang, *J. Electron. Mater.*, 2009, **38**, 1499–1503.
19 Z. Wang, A. Vemishetti, J. I. Ejembi, G. Wei, B. Zhang, L. Wang, Y. Zhang, S. Guo, J. Luo, C. Chepko, Q. Dai, J. Tang and G.-L. Zhao, *Mater. Sci. Eng., B*, 2016, **205**, 36–39.
20 Q. H. Yi Ma, B. Poudel, Y. Lan, B. Yu, D. Wang, G. Chen and Z. Ren, *Nano Lett.*, 2008, **8**, 2580–2584.
21 T. Hayashi, M. Sekine and J. Suzuki, *Mater. Trans.*, 2007, **10**, 2724–2728.
22 P. K. Nguyen, K. H. Lee, J. Moon, S. I. Kim, K. A. Ahn, L. H. Chen, S. M. Lee, R. K. Chen, S. Jin and A. E. Berkowitz, *Nanotechnology*, 2012, **23**, 415604.
23 D. M. Lee, C. H. Lim, S. Y. Shin, D. C. Cho and C. H. Lee, *J. Electroceram.*, 2006, **17**, 879–883.
24 L. Hu, H. Wu, T. Zhu, C. Fu, J. He, P. Ying and X. Zhao, *Adv. Energy Mater.*, 2015, **5**, 1500411.
25 L. Hu, T. Zhu, X. Liu and X. Zhao, *Adv. Funct. Mater.*, 2014, **24**, 5211–5218.
26 L.-P. Hu, T.-J. Zhu, Y.-G. Wang, H.-H. Xie, Z.-J. Xu and X.-B. Zhao, *NPG Asia Mater.*, 2014, **6**, e88.
27 T. Zhu, Z. Xu, J. He, J. Shen, S. Zhu, L. Hu, T. M. Tritt and X. Zhao, *J. Mater. Chem. A*, 2013, **1**, 11589–11594.
28 Z. Xu, H. Wu, T. Zhu, C. Fu, X. Liu, L. Hu, J. He, J. He and X. Zhao, *NPG Asia Mater.*, 2016, **8**, e302.
29 B. Madavali and S.-J. Hong, *J. Electron. Mater.*, 2016, **45**, 6059–6066.
30 J. L. Cui, H. F. Xue, W. J. Xiu, W. Yang and X. B. Xu, *Scr. Mater.*, 2006, **55**, 371–374.
31 W.-S. Liu, Q. Zhang, Y. Lan, S. Chen, X. Yan, Q. Zhang, H. Wang, D. Wang, G. Chen and Z. Ren, *Adv. Energy Mater.*, 2011, **1**, 577–587.
32 Z. L. Li, R. Y. Teng and S. Q. Zheng, *J. Cryst. Growth*, 2014, **406**, 104–110.
33 Z. L. Li, Y. D. Chen and S. Q. Zheng, *Nano Energy*, 2016, **28**, 78–86.
34 C.-J. Liu, G.-J. Liu, Y.-L. Liu and L.-R. Chen, *J. Mater. Chem.*, 2012, **22**, 4825.
35 Y. Zhang, G. Xu, J. Mi, F. Han, Z. Wang and C. Ge, *Mater. Res. Bull.*, 2011, **46**, 760–764.
36 L. Zhu, H. Wang, Y. Wang, J. Lv, Y. Ma, Q. Cui, Y. Ma and G. Zou, *Phys. Rev. Lett.*, 2011, **106**, 145501.
37 W. Ren, C. Cheng, Y. Xu, Z. Ren and Y. Zhong, *J. Alloys Compd.*, 2010, **501**, 120–123.
38 F. Hao, P. Qiu, Q. Song, H. Chen, P. Lu, D. Ren, X. Shi and L. Chen, *Materials*, 2017, **10**, 251.
39 S. D. Bhame, D. Pravarthana, W. Prellier and J. G. Noudem, *Appl. Phys. Lett.*, 2013, **102**, 211901.

This journal is © The Royal Society of Chemistry 2017